DISLOCATION EMISSION FROM A THREE-DIMENSIONAL CRACK — A LARGE-SCALE MOLECULAR DYNAMICS STUDY

S. J. ZHOU, D. M. BEAZLEY, P. S. LOMDAHL, A. F. VOTER, and B. L. HOLIAN

Theoretical Division and Center for Nonlinear Studies,

Los Alamos National Laboratory, Los Alamos, NM 87545

ABSTRACT

A series of massively parallel molecular dynamics simulations with up to 35 million atoms is performed to investigate dislocation emission from a three-dimensional crack. We observe dislocation loops emitted from the crack front—the first time this has been seen in computer simulations. The sequence of dislocation emission in the process of crack blunting strongly depends on the crystallographic orientation of the crack front and differs strikingly from anything previously conjectured. This finding is essential to establish a precise dislocation emission criterion (*i.e.* intrinsic ductility criterion). We also find that boundary conditions and interatomic force laws have a significant effect on jogging or blunting dislocation emission modes.

KEYWORDS

Atomistic simulation, three-dimensional crack, dislocation emission, ductility, embedded atom method

INTRODUCTION

Understanding the brittle *vs.* ductile behavior of materials is crucial to the development of new materials with high strength and toughness. Cracks and dislocations are the two major defects determining these mechanical properties. While continuum theory can successfully describe the long-range strain fields of cracks and dislocations, atomistic simulations are required to characterize their core regions. In the past, because only a small number of atoms could be simulated, various boundary treatments were employed to provide a static crack stress field [e.g., [1, 2, 3]]. In addition to their lack of dynamic response, those boundary treatments are only valid until the first dislocation travels a fraction of the computational cell away from the crack tip. Furthermore, intrinsic three-dimensional (3D) features of dislocations and cracks can not be properly investigated with only a few atoms allocated in the direction of the crack front. With the advent of massively parallel computers, simulations of many millions of atoms are now feasible [4, 5, 6, 7], allowing us to avoid using, at least for early times, complicated boundary treatments. We have developed a 3D MD code, SPaSM, (Scalable Parallel Short range Molecular dynamics) [5, 6], designed for very large scale simulations on a variety of parallel computing platforms. In addition to the computation of the many-body trajectory, SPaSM allows us to visualize, filter, and analyze the huge amount of data produced from a simulation of millions of atoms, perhaps the most challenging problem encountered in large-scale computer simulations.

To demonstrate the effectiveness of this new powerful tool and to investigate fracture behavior, we have simulated the process of dislocation emission from a 3D crack. Crack blunting by dislocation emission enhances the ductility of crystalline materials [8]. On the theoretical side, a semi-quantitative dislocation emission criterion was proposed by Rice and Thomson with continuum theory about two decades ago [8]. Recently, Rice [9] has improved this model by applying the Peierls framework (including some atomistic features into the continuum elastic theory), as has Schöck [10]. With the 2D static lattice Green's function method, Zhou et al. [11] have shown that both Schöck's and Rice's Peierls models are surprisingly accurate in describing Mode II dislocation emission from a crack, provided that some modifications are made. However, it is found that the tensile effects associated with breaking of bonds must be included for a satisfactory description of Mode I dislocation emission (i.e., edge dislocations are emitted on a plane inclined to the crack plane) [12]. With the variational boundary integral method, Xu et al. [13] have further investigated the critical configuration for nucleation of dislocations from crack tips. Undoubtedly these existing theories and models are helpful in understanding brittle vs. ductile behavior to some extent, but a more realistic criterion must incorporate atomistic information about dislocation emission from a 3D crack. On the experimental side, it is still a challenging task to observe the dynamic and three-dimensional process of dislocation emission from a crack tip, even though experimental techniques such as High Resolution Transmission Electron Microscopy are getting more powerful. Therefore, it is necessary to perform large-scale MD simulations to obtain information which is inaccessible to experiment.

There are two kinds of 3D dislocation emission processes: blunting and jogging. In the blunting configuration the dislocation is on a slip plane inclined to the crack plane and containing the crack front. The emission causes the crack to blunt in the direction of the Burgers vector **b**. In the jogging configuration, the slip plane is oblique to the crack front, and the emission makes a jog in the crack front in the direction of **b**. Blunting lowers the stress concentration at the crack front and hinders the propagation of the crack, thus making the material tough. The effect of jogging on crack propagation is relatively small. The jog is a dragging point for the crack, but may not be a major contributor to toughness. In addition to these geometrical changes, dislocation loops also shield or antishield cracks (i.e., reduce or increase the stress intensity factor at the crack tip). The driving force for emission of a blunting dislocation is large because a flat dislocation loop can release more strain energy by being as close to the crack front as possible [17]. On the other hand, there is probably less resistance to the emission of a jogging dislocation, since it does not create new surface like the blunting dislocation. While both jogging and blunting dislocations have been observed in experiments [14, 15], the theoretical picture is much less clear [16, 17, 18, 19, 13]. Argon [16] has first called attention to the possibility that jogging dislocation emission may be easier than blunting. Schöck [18] has recently calculated the energy of a shear dislocation loop in the framework of the Peierls model and suggested that the barrier for jogging dislocation emission is comparable to that for blunting dislocation emission. However, the problem is getting even more complex, considering the fact that in real (3D) materials crack-tip fronts are not always straight, even in a pure Si single crystal. Zhou and Thomson [17] proposed that ledges (i.e. cleavage steps) on crack fronts can serve as "easily operated" dislocation nucleation sources, as confirmed experimentally a few years later by George and Michot [20]. Xu et al. [13] have recently found by evaluating the activation energy for dislocation emission that the order of ease of dislocation emission in α-iron proceeds as: (1) ledge with sufficient height; (2) blunting; and (3) jogging. But it is known that continuum theories or hybrid continuum approaches are not accurate in describing highly nonlinear, dynamic, and atomistic processes such as dislocation emission from a crack tip; therefore their estimates of the energy barriers for dislocation nucleation are questionable. Furthermore, these calculations of dislocation nucleation from a ledge actually ignore the effect of ledge corners, which, due to their high stress concentrations, could be the preferred site for dislocation nucleation (see Zhou and Thomson [17]). In this paper, we present computer experimental results that shed light on the sequence of 3D dislocation emission events at straight crack tips.

SIMULATION RESULTS AND DISCUSSION

In our MD simulations the atoms interact either via Morse pair potentials, differing in stiffness parameter, α, or via a more realistic embedded atom method (EAM) potential for copper. The EAM, a many-body form in which a pairwise interaction is augmented with a term dependent on the local atomic density [21], has been shown to provide a good description of transition metals, especially those with filled or nearly filled d shells [22, 23]. The Cu potential employed here was fit to the bulk lattice constant, cohesive energy, elastic constants and vacancy formation energy, as well as the bond energy and bond length of the gas phase copper dimer, as described elsewhere [24, 25]. The cutoff distance, for both the pair and density functions, is between the third- and fourth-nearest-neighbor distance in the equilibrium face-centered-cubic (fcc) crystal. Throughout, we use as units the atomic mass m, distance r_o between nearest neighbors in the zero-temperature and zero-pressure crystal, and bond energy ε; hence the unit of time t_0 (~ 2.5 vibrational periods, or $\sim 10^{-12} sec$) is given by $\varepsilon = m r_0^2/t_0^2$; the time step is $0.01 t_0$. In these units, the Morse pair potential is written as $\phi(r) = e^{-2\alpha(r-1)} - 2e^{-\alpha(r-1)}$ with a cutoff at $r_{max} = 2.5 r_o$.

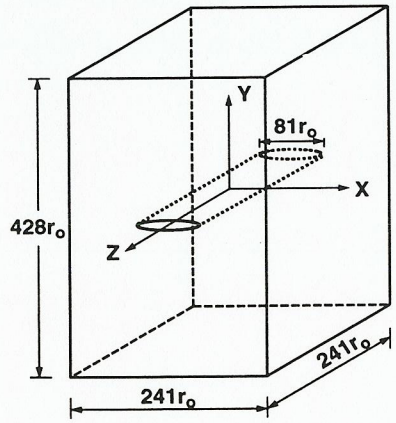

Fig. 1: Schematic of the molecular-dynamics computational cell for 35 million atoms. Periodic boundary planes: xz and yz; free surface planes: xy. The shortest distance between periodic-image crack tips is 160 r_o, requiring a time of $\sim 30 t_o$ for sound-wave communication.

In this paper, we will concentrate on exploring mechanical aspects of dislocation emission without thermal fluctuations, so we set the initial temperature to nearly zero ($10^{-6}\epsilon/k$). A schematic of the MD system is shown in Fig. 1. The atoms are initially placed in perfect fcc crystal lattice sites. Dislocation emission from a crack is relatively easy in

fcc crystals, and interatomic potentials for fcc metals are well characterized. The crystal orientation of our fcc system is shown in Fig. 2, including the (010) xz crack plane and {111} slip planes. In fcc metals of relatively low stacking fault energy, including copper, slip dislocations on the close-packed {111} planes are in extended configurations, consisting of two Shockley partial dislocations separated by a stacking fault ribbon (see Fig. 3). In our MD simulations, we use a large computational cell with periodic boundary conditions in the $x-$ and $y-$directions to keep the long-range character of the crack and dislocation strain fields. We save computation time by initially embedding an atomistically sharp equilibrium crack (loaded at the Griffith critical strain ϵ_c), displacing atoms according to the continuum elastic solution for a finite crack in an unbounded solid. System sizes ranged from 1.7 to 35 million atoms (see Fig. 1). Various numbers of planes were chosen in the z direction to explore 3D effects. The shortest half crack-length of the sharp initial crack was $20r_o$, which is long enough to have the crack strain field be close to that of a continuum crack. We produce a crack that initially lies on the xz plane under uniaxial remote loading strain ϵ_o (just below ϵ_c) in the y-direction (see Fig. 1). We gradually increase the loading strain by applying a homogeneous strain rate, where the xz periodic boundary planes move apart from each other at constant velocity. The atoms first readjust their initial positions given by elastic theory, ending up with more rounded crack tips. The crack extends forward by no more than two lattice spacings, whereupon dislocation loops are eventually nucleated without further crack extension.

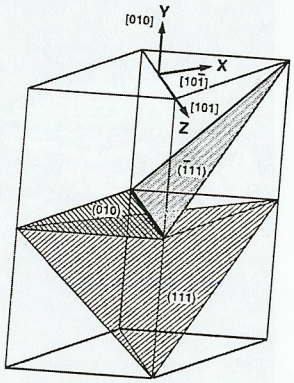

Fig. 2 : Crack-slip plane geometry. The crack plane is on (010) and crack front is along [101]. One set of {111} slip planes, e.g. ($\bar{1}$11), contains the crack front and the others, e.g. (111), do not.

For a 3D crack at equilibrium, the vicinity of a free boundary surface normal to the z-axes is under plane stress: the stress $\sigma_{zz} = 0$ and the strain $\epsilon_{zz} \neq 0$; while the bulk is under plane strain: the displacement $u_z = 0$. According to linear elastic fracture mechanics, the maximum shear stress under plane stress is at planes through the x axis subtending an angle of 45° with the xz plane, but the maximum shear stress under plane strain is not only much lower than that under plane stress, but also on different planes, through the z axis at 45° from the xz plane [26]. Thus, the mode and threshold stress for dislocation emission from the junction between the crack front and the free surfaces is expected to differ from the bulk. The strain ϵ_{zz} is zero and therefore the stress σ_{zz} is *not* zero in our

initial set up (at $t = 0$). For $t > 0$, free surface boundaries induce a dynamic transition region between surface and interior. Tensile (Mode I) loading ($\sigma_{yy} > 0$) induces a Poisson-ratio contraction in the vicinity of the free surface, which is magnified near the junction with the crack tip. Figure 4a clearly shows that regions near the junction are indented, but those near the crack surfaces bulge out. The dynamic contraction, combined with the plane stress condition, punches jogging dislocations out from junctions. The half-loop dislocations are approximately mirror-symmetric with respect to the xz crack plane, pinning on the free surfaces, as shown in Figs. 4a, 4b, and 5a. Note that these jogging dislocation loops exhibit a bent "<" shape, where one jogging loop is above the crack front while the other is roughly mirror-symmetric below, rather than a straight "\" shape, as previously conjectured [16, 17, 18, 13] (see Figs. 4a, 4b and 5a). Similar jogging dislocation emission from junctions has been observed experimentally in silicon [20].

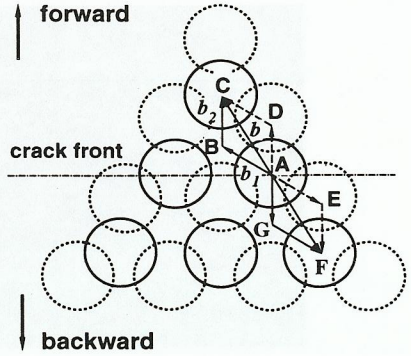

Fig. 3 : Two atomic layers of a {111} slip plane show the permitted pathways of the forward ($A \rightarrow B \rightarrow C$) and backward ($A \rightarrow G \rightarrow F$) motions, relative to the crack propagation direction, for the perfect dislocation. Motion from A to D or from A to E is energetically forbidden by the existence of atoms D and E. The perfect dislocation with Burgers vector $b = 1/2[01\bar{1}]$ and its two partial dislocations with Burgers vectors $b_1 = 1/6[\bar{1}1\bar{2}]$ and $b_2 = 1/6[12\bar{1}]$ are shown. For a unit length of dislocation, the driving force is $\mathbf{F} = (\mathbf{b} \cdot \sigma) \times \xi$, where σ is the stress tensor, and ξ is the unit vector describing the dislocation line direction. For blunting dislocation emission, $F = b_r \sigma_{r\theta}$, where b_r is the radial component in the xy plane of $\mathbf{b}$ and $\sigma_{r\theta} \propto \sin(\theta/2)\cos^2(\theta/2)$. The angles θ between the inclined {111} slip plane and the crack plane are 54.73° and 125.27° for forward and backward partial dislocation emission, respectively. Therefore $F_{backward}/F_{forward} = 1.034$.

We have overcome the challenging problem of visualizing these dramatic 3D phenomena inside our large computational cells by noting that the potential energies of individual atoms near free surfaces and dislocation cores are narrowly peaked at values above the cohesive (bulk) energy (about -6ε in fcc). Thus, we can select potential values within certain ranges about those peak values to render bulk atoms invisible and display the structures of dislocation loops, for example. For the Morse potential with stiffness parameter $\alpha = 7$, under free surface boundary conditions, we observe only jogging dislocation emission from the crack front (see Fig. 5a). On the other hand, we find that under periodic boundary conditions, the crack tends to emit dislocations while deflecting (branching) from the initial {100} plane to a {111} plane, which has a lower surface energy (see Fig. 5b). Hence, we

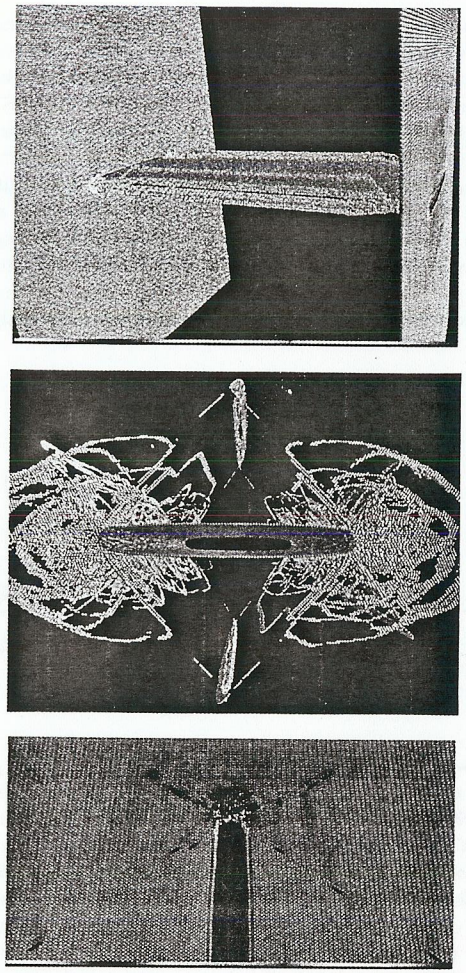

Fig. 4: Blunting dislocation loops emitted backward from the crack front and jogging dislocation loops generated from the junctions between free surfaces and the crack front: 35 million atoms interacting via EAM Cu potential. The strain rate is 0.001 t_0^{-1} (about 10^9 sec^{-1}). Particles are colored by atomic potential energy; to visualize dislocation loops and the crack front, only particles with atomic potential energy between -5.89ε and -3.8ε are shown. (With this potential energy selection, we effectively reduce the 700 MB original data by a factor of ∼ 80.) (a) the first backward dislocation emission ($t = 9.5t_0$); (b) The dislocation loops in the region after removing free surfaces, viewed along the crack front ($t = 25t_0$). (c) the emission sequence shown in the $z = 0$ plane ($t = 25t_0$). Note possible Lomer dislocations ($1/2[10\bar{1}]$ on (010)), emitted from both lower and upper edges of the blunted crack.

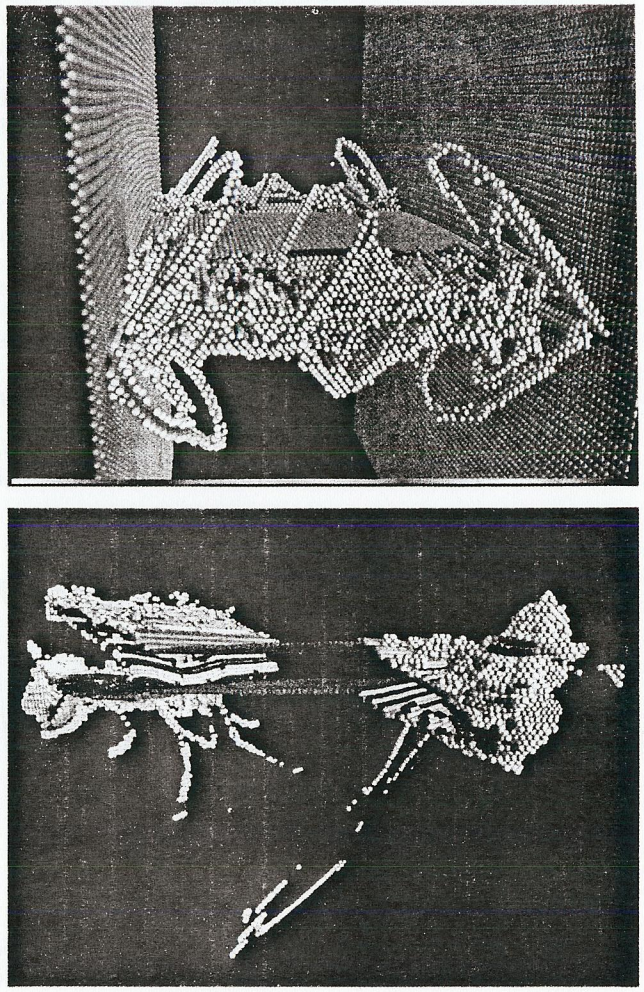

Fig. 5: The effects of boundary conditions in the z direction. 1.78 million atoms interacting via a Morse potential ($\alpha = 7$). The strain rate is $0.0002\,t_0^{-1}$. Only particles with atomic potential energy between -6.08ε and -2.0ε are shown. (a) Under free boundary conditions, jogging dislocation loops are generated from junctions as well as the crack front ($t = 12t_0$). (b) Under periodic boundary conditions, cracks branch (i.e. deflect) from the original (010) crack plane onto {111}-type planes, and emit blunting half-dislocation loops along {111} planes ($t = 13.0t_0$).

believe that $\alpha = 7$ is a borderline case between ductile and brittle fracture. For $\alpha = 6$, a flat, long blunting dislocation is first emitted from the crack front, and then many jogging dislocations are ejected along it. In contrast, we observe only blunting dislocation emission along the crack front in EAM Cu (see Fig. 4a), where the central region is still straight after being blunted by dislocation emission, except at the points where the dislocation loop is pinned. The crack front near a free surface, however, is seriously disturbed by jogging dislocation emission. In general, the shorter the range of an interatomic potential, the harder it is to emit blunting dislocations (see [11, 12, 7]). For dislocation emission in EAM Cu, blunting is easier than jogging; thus, jogging only occurs at the junction. For Morse $\alpha = 7$, blunting dislocation emission is difficult, and therefore jogging dislocations are emitted all along the crack front. Ledge formation energy as a function of interatomic potential may provide a clue to understanding this switch of the dislocation emission mode.

We see the same features in the process of blunting dislocation emission in EAM Cu simulations of 35 million and 3.5 million atoms (differing by a factor of 2 in crack length and factors of 2, 2.5, and 2 in $x-$, $y-$, and z-lengths, respectively). We therefore conclude that 3.5 million atoms is sufficiently large for realistic investigation of 3D dislocation emission, at least at the early stage. In our 35 million atom system, there are 241 planes in the z-direction, so that there is no intrinsic restriction on 3D dislocation emission, in contrast with previous quasi-3D simulations with a periodic thickness of two atomic layers [1, 2, 27]. Dislocation emission processes occur above and below the crack tip roughly in the same sequence and at the same time for both system sizes. We observe that a half-loop Shockley partial dislocation emerges at $t = 5.5t_0$ on {111} slip planes, which is very long ($\sim 190r_0$) and flat in the direction of the crack front. This indicates that a minimum length of crack front is required to accommodate the first blunting dislocation emission.

Surprisingly, the first partial is ejected backward (see Figs. 3 and 4). Next, a second partial is emitted *forward* at $0.5t_0$ later. One might suppose that because the stress in the forward direction is higher than that in the backward, the first partial should be emitted in the forward direction. However, the driving force on the dislocation depends on the product of the stress and the Burgers vector. The pathways for forward and backward emission are shown in Fig. 3. The driving force for backward motion of the partial with b_2 is only about 3% larger than that for forward motion of the partial with b_1. With an anisotropic crack stress field, this ratio becomes about 1.30 [27]. This calculation, based on a rough continuum approximation, is consistent with the observation that the second partial dislocation is emitted forward soon after the first partial is emitted backward, which we have confirmed by performing the Burgers circuit around the partials. Using quasi-3D MD, Hoagland [27] observed backward dislocation emission in EAM Ni, while deCelis et al. [2] report that two Shockley partial dislocation *lines* were emitted *forward* at $T = 300°K$ for Cu. Schiøtz et al. [28] report that extended dislocation loops are emitted forward from a wide notch in their 3D MD simulations in Cu. (However, since the two notch surfaces are chosen to be {111} slip planes, their simulations artificially forbid backward emission.) Gumbsch and Beltz [29] also observed the backward dislocation emission in their quasi-3D molecular statics simulation in EAM Ni.

It is even more striking to see that the other two partials with b_2 (the same type as the first one) are later emitted backwards in different adjacent {111} slip planes, leaving behind a twin (see Fig. 4c). With the simulations continuing up to $t = 25t_0$, we did not observe the backward emission of an extended dislocation. Under the condition of no external stresses,

the calculated equilibrium separation r_e between these two Shockley partials is about 5.7 nm ($22r_0$) for EAM Cu. However the separation for the two partials just emitted from the crack front could be quite different from r_e due to the strongly varied stress field around the crack tips and interactions with other emitted dislocations. It is likely that the backward emission of an extended dislocation would be observed in a larger computational system at longer times. Because enlarging the separation between two partials increases the stacking fault energy, this increases the driving force for the emission of the second partial and could eventually drive the second partial out of the crack front. Aside from the Shockley partial emission, we also observe emission of Lomer dislocations, for which the high deformation ahead of the blunted crack tip could provide the local driving force (see Fig. 4b).

CONCLUSION

With these large-scale MD simulations in 3D, we have observed for the first time unambiguous evidence of emission of blunting and jogging dislocation loops. These three-dimensional dislocation phenomena can effectively be visualized and analyzed by a new technique, where only those atoms within certain ranges of atomic potential energy are plotted. Our calculations have shown that the dynamic sequence of emission correlates well with energetic analysis, but differs significantly from previous conceptualizations of these processes.

ACKNOWLEDGMENT

Computations were performed on the TMC CM-5 and CRAY T3D at the Advanced Computing Laboratory (ACL) at Los Alamos. We also thank Robb Thomson, Ali Argon, John Hirth, Richard Hoagland, and Peter Gumbsch for helpful discussions.

References

[1] R. G. Hoagland, P. C. Gehlen, and J. P. Hirth, Phil. Mag. **34**, 413 (1976).

[2] B. deCelis, A. S. Argon and S. Yip, J. Appl. Phys. **54**, 4864 (1983).

[3] K. S. Cheung and S. Yip, Phys. Rev. Lett. **65** 2804 (1990).

[4] B. L. Holian and R. Ravelo, Phys. Rev. B **51**, 11275 (1995).

[5] P. S. Lomdahl, P. Tamayo, N. Grønbech-Jensen, and D. M. Beazley, *Proc. of Supercomputing 93*, IEEE Computer Society Press, p. 520-527 (1993).

[6] D. M. Beazley and P. S. Lomdahl, Parall. Comp. **20** 173 (1994).

[7] S. J. Zhou, P. S. Lomdahl, R. Thomson, and B. L. Holian, Phys. Rev. Lett. **76**, 2318 (1996).

[8] J. R. Rice and R. Thomson, Phil. Mag. **29**, 73 (1974).

[9] J. R. Rice, J. Mech. Phys. Sol. **40**, 239 (1992). **47** 7710 (1994).

[10] G. Schöck, Phil. Mag. A **63**, 111 (1991).

[11] S. J. Zhou, A. E. Carlsson and R. Thomson, Phys. Rev. B. **47** 7710 (1994).

[12] S. J. Zhou, A. E. Carlsson and R. Thomson, Phys. Rev. Lett. **72**, 852 (1994).

[13] G. Xu, A. S. Argon, and M. Ortiz, Phil. Mag. **72**, 415 (1995); G. Xu, A. S. Argon, and M. Ortiz, to be published.

[14] K. Y. Chia and S. J. Burns, Scripta Metall. **18**, 467 (1984).

[15] Y.-H. Chiao and D. R. Clarke, Acta. Metall. **37**, 203 (1989).

[16] A. S. Argon, Acta. Metall. **35**, 185 (1987).

[17] S. J. Zhou and R. Thomson, J. Mater. Res. **6**, 639 (1991).

[18] G. Schöck and W. Puschl, Phil. Mag. A **64**, 931 (1991); G. Schöck, Phil. Mag. in press.

[19] J. R. Rice and G. E. Beltz, J. Mech. Phys. Solids **42**, 333 (1994).

[20] A. George and G. Michot, Mater. Sci. and Eng. **A164**, 118 (1993).

[21] M. S. Daw and M. I. Baskes, Phys. Rev. B **29**, 6443 (1984).

[22] M. S. Daw, S. M. Foiles, and M. I. Baskes, Mater. Sci. Reports **9**, 251 (1993).

[23] A. F. Voter, in *Intermetallic Compounds: Principles and Practice*, edited by J. H. Westbrook and R. L. Fleischer, John Wiley and Sons, Ltd, 1994), Vol. 1, p. 77.

[24] A. F. Voter and S. P. Chen, Mat. Res. Soc. Symp. Proc. **82**, 175 (1987).

[25] A. F. Voter, Los Alamos Unclassified Technical Report #LA-UR-93-3901.

[26] D. Broek, *Elementary Engineering Fracture Mechanics*, Martinus Nijhoff Publishers, Boston, 1982.

[27] R. G. Hoagland, *Proc. of the Symposium on New Techniques for Characterizing Corrosion and Stress Corrosion*, TMS, Cleveland, 1995.

[28] J. Schiøtz, K. W. Jacobsen, and O. H. Nielsen, Phil. Mag. Lett. **72**, 245 (1995).

[29] P. Gumbsch and G. E. Beltz, Modelling Simul. Mater. Sci. Eng. **3**, 597 (1995).